RSC Advances

ROYAL SOCIETY OF CHEMISTRY

www.rsc.org/advances

Charge Heterogeneity Induced Binding and Phase Stability in β-lacto-globulin-Gelatin B Gels and Coacervates at their Common pI

Jyotsana Pathak[1] , Kamla Rawat[2*] and H. B. Bohidar[1,2*]

[1]Polymer and Biophysics Laboratory, School of Physical Sciences,

Jawaharlal Nehru University, New Delhi 110067, India

[2] Special Center for Nanosciences,

Jawaharlal Nehru University, New Delhi 110067, India

*Corresponding authors email: bohi0700@mail.jnu.ac.in, kamla.jnu@gmail.com

Tel: +91 11 2670 4699, Fax: +91 11 2674 1837

Abstract

An understanding of the interactions between Gelatin B (GB) and β-lacto-globulin (β-Lg) mainly arising from surface selective patch binding occurring at their common pI (≈5.0±0.5) in the absence of added salt. Heterogeneous surface charge distribution on β-Lg facilitated such interaction at different mixing ratio ([GB]: [β-Lg] = r) and the GB-β-Lg complexes carried distinctive surface charge (seen through their zeta potential, ζ). For r < 1:1 (partial charge neutralization, ζ ≈0) a turbid solution was formed which gives the indication of formation of intermolecular soluble complexes. For r > 1:1 (overcharged regime, ζ > 0) the dispersion remained transparent and homogeneous which gives no phase separation, but the dispersion formed a gel on waiting. The overcharged gels were homogeneous, more rigid and higher melting temperature in comparison to coacervate. In the coacervate phase, the intensity of the scattered light I_s, and its time-correlation function $[g_2(t)-1]$ did not evolve with time. In contrast, the gel phase displayed considerable change with aging time t_w. For gels, as $t_w \rightarrow \infty$ the system moved from ergodic to non-ergodic state. At $t_w=0$, the correlation function exhibited one relaxation mode due to the system residing deeply inside the ergodic phase and purely mirroring Brownian dynamics. After a characteristic waiting time, t_w an additional mode (slow relaxation) appeared which was attributed to inter-chain interaction induced reorganization of entanglements. This characteristic time was the time required for the system to get dynamically arrested, similar observation was made from rheology measurements too. A comprehensive phase diagram depicting the stability of the dispersion in various charged soft matter states of the complex under various temperature conditions was established.

Key words: Gelatin B, β-lacto-globulin, protein-protein binding, non-ergodicity, dynamic light scattering.

1. Introduction

Protein-Protein interaction is very strongly dependent on reaction environment like, the pH, ionic strength, temperature, protein surface charge distribution, protein structure etc. The heterogeneous surface charge distribution on near globular proteins[1] like bovine serum albumin (BSA), β-lacto globulin (β-Lg), human serum albumin (HSA) etc make their interaction with polyelectrolytes in general and polyampholytic proteins like gelatin, in particular quite interesting[2-4]. The inter-protein interaction at their common pI is very revealing because such interactions are sometimes governed by a lesser known interaction called surface patch binding (SPB)[2]. Unlike electrostatic interaction where associations are dominated by net charge on oppositely charged protein molecules, SPB interactions can prevail even when the net charge on both proteins is of same. It has been realized in many biological assembly that SPB type interactions cause intermolecular association leading to soluble complex formation[3-11]. The heterogeneous surface charge distribution on one of the protein molecules, and the small persistence length of its binding partner offer adequate possibility for the surface selective binding to take place where the chain segment of the polyampholyte molecule intelligently chooses the oppositely charged patch on the other protein overcoming the repulsion between the similarly charged chain segment and surface patch of the colloidal protein molecule[12]. Therefore, for SPB interactions to be relevant, it is imperative to have a pair of proteins where one is a colloidal protein molecule (like BSA, HSA, β-Lg etc) and the other is preferably a low persistence length polyampholyte (like gelatin A and gelatin B). In general, there can be another scenario where a pair of biopolymers is chosen with one component being a polyelectrolyte (like agar, chitosan, DNA etc) and another flexible chain polyampholyte. Experiments have shown that in both the aforesaid cases SPB interactions have yielded soluble intermolecular complexes

that eventually lead to liquid-liquid phase separation giving rise to complex coacervation[9]. Complex coacervation is a first-order thermodynamic phase separation caused due to associative interaction between a pair of oppositely charged polyelectrolytes, or a colloid-polylectrolyte pair. The partial charge neutralization caused due to binding between the two components (in coacervates), release of counter-ions and the random mixing of the components drives the phase separation[13-14]. Several theoretical models have been proposed to account for this phenomenon[15-27].

Protein based coacervation, transition is driven by surface selective patch binding even though both the biopolymers carry similar net charge[28,30] and some other Protein based coacervates, which is formed by strong electrostatic interactions, has been reported for β-lacto-globulin- Gum Arabic[30-32], whey protein-gum Arabic[33-34], gelatin-chitosan[35], gelatin-agar[36], gelatin-gelatin[36], gelatin- DNA[38] and β-lacto-globulin-pectin systems[39]. Whey protein-gum arabic coacervate was observed to be a highly concentrated solution phase (melt-like) whereas the diversity of material properties associated with coacervates β-lacto-globulin-gum arabic coacervates were found to be associated with vesicular to sponge-like internal structure. In contrast, β-lacto-globulin-pectin coacervates were found to be a heterogeneous phase comprising of pectin networks with protein domains forming the junction points[39]. It has been reported that a polyelectrolyte, DNA and a polyampholyte, gelatin B can undergo associative interactions and form complex coacervates with interesting thermal properties[38].

A lesser observed phenomenon is network formation between the complementary biopolymer pair leading to gelation transition. The interpenetrating network structure plausibly formed due to self-assembly of the biopolymers results in a viscoelastic phase where the solvent gets trapped as interstitial fluid. The soft matter phase of biopolymers, gels and coacervates, are

thermodynamic states that are distinctively different from the point of their self-assembly, and their structural evolution with time. The complexity of phase diagram that describes the co-existence of the two interacting biopolymers arises from the fact that continuous reorganization of the relative assembly of the constituents can give rise to physical states that are hierarchical in concentration. Therefore, length and time scales become relevant. This aspect of soft matter science in general, and in protein-based soft materials, in particular, has been poorly reported in the literature. Herein, we probe this dynamics in finer details and show that GB- β-Lg based system exhibits charge heterogeneity induced binding, phase stability and anomalous relaxation in gels and coacervates at their common pI.

2. Material and Methods

The sample used in this study is bovine extracted gelatin B (GB, bloom 225 and molecular weight 100 kDa) and β-Lg a globular protein (molecular weight 67 kDa) were bought from Sigma-Aldrich chemical company (U.S.A.), in which according to supplier had a minimum purity of > 98%. It needs to be mentioned that the proteins were not subjected to further purification by dialysis, which would have made these salt free. The two proteins which is used in this study are known to have a common pI= 5.0±0.2[38]. All concentrations are in used in % (w/v) unless otherwise stated.

The aqueous solution of β-Lg was prepared by dissolving known fix amount of the protein 0.75 % powder in double distilled deionized water at 25 ^{0}C using a magnetic stirrer for about 30 min. The aqueous solutions of GB were prepared at concentrations of 0.25-4.00 % by dissolving known amount of the protein powder in double distilled deionized water at 40 ^{0}C using a magnetic stirrer for about 1.5 hours. These stock solutions appeared optically clear to the

eye and all measurement procedures were performed at room temperature 25 ^{0}C. Relative humidity in the laboratory was close to 50%.

The stock samples as β-Lg and GB stock solutions were prepared by mixing the two in the following ratios: r = [GB] : [β-Lg] = 0.25:0.75, 0.50:0.75, 0.75:0.75, 1:0.75, 2:0.75, 3:0.75 and 4:0.75. The GB: β-Lg ratio is defined 0.33, 0.66, 0.75, 1, 1.3, 2.6, 4, 5.3 parts of GB mixed with as 0.75 part of β-Lg (v/v) respectively. All complex coacervate samples were prepared by mixing the two stock solutions in a fix volumetric ratios, r = 0.25:0.75, 0.50:0.75 and 0.75:0.75. All mixture of solutions was then titrated with 0.1N HCl or 0.1N NaOH to adjust the pH to pI. These samples were stored in air tight borosilicate glass bottles (trace amount of sodium azide was added to the samples to prevent bacterial contamination) for further analysis. Coacervates were extracted from mixed solutions following standard procedure of repeated centrifugation and decantation of the supernatant[40-43]. These samples were stored in airtight borosilicate glass bottles to form gels, and for their subsist analysis, which, in all instances, did not exceed more than 24 h of preparation.

Zeta potential (ζ) measurement was performed on both coacervate and gel samples with an electrophoresis instrument (model: ZC-2000, Microtec, Japan). The electrophoretic cell was made of Teflon (dimensions 140mm$W$ × 40mm$D$ × 60mm$H$) with distance between electrodes fixed at 10 cm. In all our measurements the migration voltage was fixed at 25mV. The instrument was calibrated against 10−4M AgI colloidal dispersions. More details of Zeta potential are given in ref. [28-29]. Dynamic light scattering (DLS) experiments were performed at a scattering angle of θ = 90^0 and laser wavelength of λ = 632.8 nm on a 256 channel digital correlator, (PhotoCor Instruments, USA) that was operated in the multi-τ mode (logarithmically spaced channels). Robustness of the fitting results was decided based on two criteria: sample to

sample accuracy, and data reproducibility within the same sample. Further information on this set up is provide in ref.[38-45]

Rheology is the study of flow and deformation of materials under applied forces. Rheology measurements performed on the both samples (coacervate and gel), using small amplitude oscillatory shear, were performed on controlled stress AR 500 rheometer (TA Instruments, Surrey, England). Measurements were carried out with a cone plate geometry (2^0) using a controlled stress was 1 Pa and a fixed angular frequency of 1Hz. Temperature dependence of dynamic storage modulus was recorded by heating the samples from 20 to 50 ^{0}C in the ramp mode. More details are available in ref.[46-47].

3. Results and Discussion

At low mixing ratio r>1 of β-Lg and GB solution, the mixture appears turbid, which gives the indication of formation of intermolecular soluble complexes, finally leading to phase separation, called coacervation[41-43] while at high mixing ratio r<1 the mixture turns transparent with no indication of either insoluble complex formation or phase separation, but the mixture turned into a gel like phase over time. It was possible to distinguish between the properties of all low mixing ratio samples (coacervate) and high mixing ratio samples (gel) samples conclusively from the following experiments.

The simplest binding profile showed clearly distinguishable regions in zeta potential and absorbance profile (Fig. 1). Absorbance profile, which was obtained from the analysis of the change in the slope of the absorbance (at λ=290 nm) as a function mixing ratio (r) plot is shown in Fig. 1(b). Change in slope identifies two phases; one is coacervate, and other is gel which will be discussed later. In zeta potential profile is shown in Fig. 1(a). For r < 1.0, the ζ potential of the

complexes of β-Lg and GB increased from (−6) to 0 mV, which was assigned to the coacervate phase (complete charge neutralization); this was evident from increase in solution turbidity (Region-I), and for r > 1.0 the complexes of β-Lg and GB were found to be positively charged, and the solution was transparent (+ve zeta potential, overcharging, Region-II).

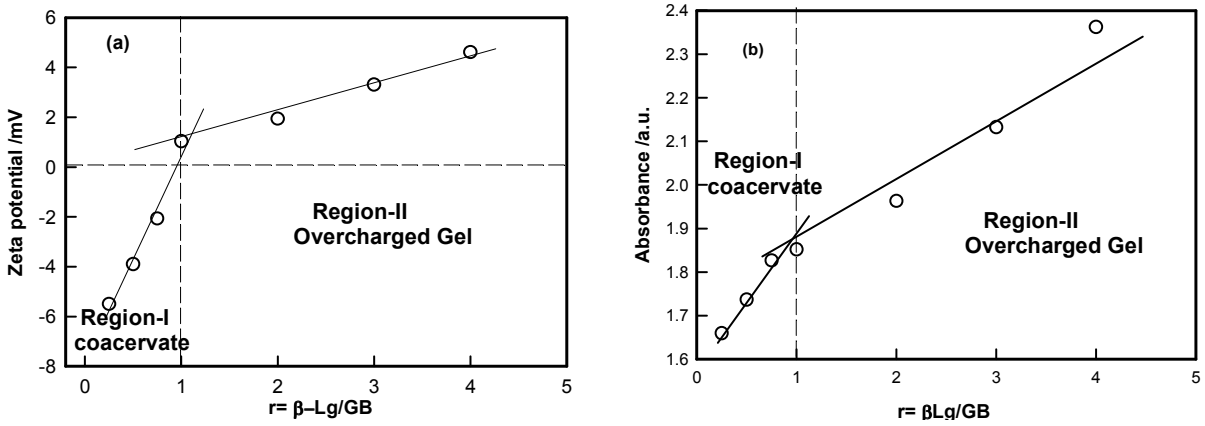

Figure 1: Typical measured (a) zeta potential and (b) absorbance as a function of mixing ratio r. Note that the soluble complexes in Region-I were either partially or fully charge neutralized while in Region-II, these were overcharged. Subsequently, these two regions yielded complex coacervates and transparent overcharged gels. See text for details. Solid lines are guide to the eye only.

3.1. Viscoelastic properties

The viscoelastic properties of all samples were characterized by rheology. Fig. 2 represents the temporal evolution of *G*' for all the samples. The highest *G*' value was obtained for at *r* = 5.3. These gels were transparent and formed rapidly, possibly due to the increased viscosity of the system, which resulted in the reduced motility of the complexes. The gelation time t_g obtained from the G' data depicts an initial growth regime followed by a plateau. For r = 2.6 and r = 4.0 samples the low G' values were substantially low (15-25 Pa) where as for r = 5.3 sample yielded

G'= 45 Pa. For r = 1 there was no observation of gelation which is clearly seen from Fig. 2. We identify two phases (i) sol phase, ($t < t_g$), storage modulus increased in a linear way and (ii) Gel phase ($t > t_g$) storage modulus remained invariant of time.

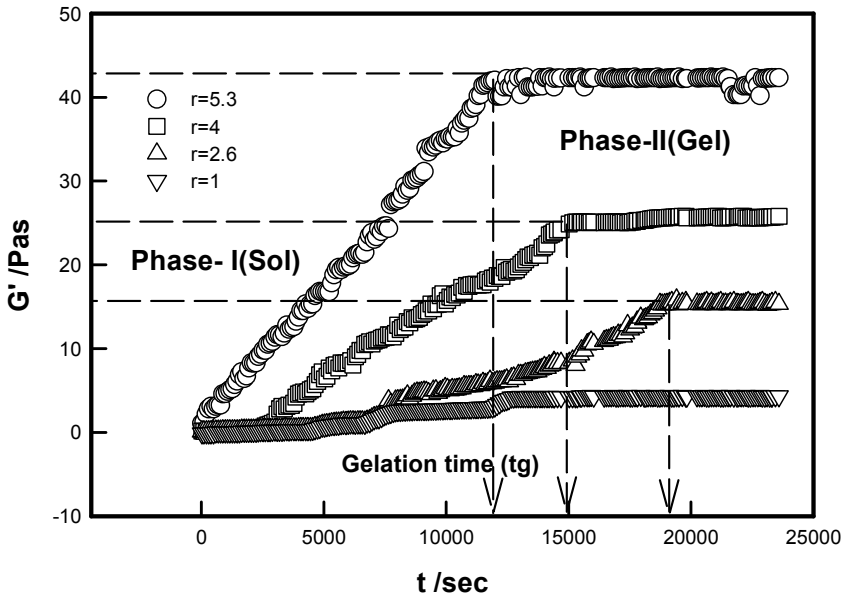

Figure 2: Variation of viscoelastic **s**torage modulus (G') as function of time during gelation of β-Lg/GB sol shown for r = 1.0, 2.6, 4.0 and 5.4. The measurements were performed at 25 ^{0}C using a constant oscillation stress of 1 Pa**.** The dotted line represents the gelation time t_g. See text for details.

It was observed that the GB with β-Lg dispersion in water formed viscoelastic gels over a range of concentration. The profiles of storage modulus (G') and loss tangent as a function of frequency for gel and coacervate is shown in Fig. 3. The typical storage modulus, G'(ω) , defined as the energy stored in the system at a given temperature whereas the loss factor tan δ reveals the ratio between the viscous and the loss portion of the deformation behavior. In viscoelastic

systems, relation between the frequency dependence of the elastic moduli near gelation[47,48] given by is

$$G'(\omega) = S\omega^{n'}, \qquad 0 < n < 1 \tag{1}$$

$$G''(\omega) = S\omega^{n''}, \qquad 0 < n < 1 \tag{2}$$

and $$G'(\omega)/G''(\omega) = \tan\delta = \tan(n\pi/2) \tag{3}$$

where S defined as elastic strength of the material and n is the relaxation exponent, it is assumed that there is no universal value of n, because n is related to the specifics of each gelling system. The linear viscoelasticity theory[50,51] applicable for both pre and post gel conditions and predicts the stress– relaxation to follow the power-law frequency dependence behavior given by eqn (1) with $0 < n' < 1$. Stoichiometrically balanced and imbalanced cross-linked networks showed n = 1/2 (excess cross linking) and n > 1/2 (deficient of cross linking) respectively. Thus, it is useful to define the dispersion relation in a more generalized form as: $G'(\omega) \sim \omega^{n'}$ and $G''(\omega) \sim \omega^{n''}$. The least-square fitting of the data to this equation yielded $n' = 0.21 \pm 0.01$ invariant of mixing ratio for gels. For coacervate samples $n' = 0.14 \pm 0.01$. This indicated that gel samples were more viscoelastic than coacervates Fig. 3(a).

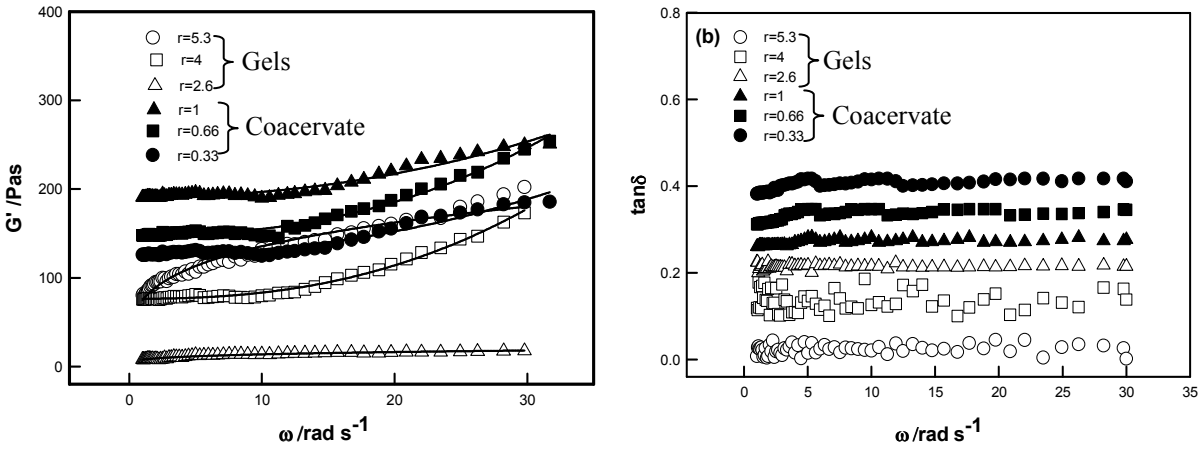

Figure 3: Evolution of (a) storage modulus G′(ω) and (b) loss tangent of coacervate and gel samples with respect to angular frequency. All measurements were performed at 25 ^{0}C using constant oscillation stresses of 1 Pa. Solid lines in (a) is fitting for equation (1).

The elastic attribute of the coacervates was felt pertinent to resolve whether or not these had gel-like structures. For determining this, the loss tangent $\left(tan\delta = {}^{G''}/_{G'}\right)$, was plotted with respect to frequency, which is illustrated in Fig. 3(b), For gel state the tan δ versus ω slope is positive, whereas at the point of gelation it is zero while it is negative for melt state[51,52]. Fig. 3(b), indicates that the loss tangent with respect to ω is associated with a small positive slope implying that the coacervate material was indeed gel-like. When tan δ < 1 (G'> G"), which confirmation of the solid-like attribute of the material. On the contrary, when tan δ > 1, liquid-like behaviour prevails. In the present system tan δ of coacervate was consistently higher value than tan δ of gels which confirms more fluidity of the coacervate state compared to the gel state samples.

In the gel state, water is available as interstitial water trapped inside the network or hydration water attached to the networks. In contrast, in coacervates, most of the water is attached to the intermolecular complexes as hydration water. The coacervates samples comprise of a heterogeneous phase with localized finite size networks embedded in an assembly of randomly mixed intermolecular complexes.

The melting profile of coacervate and gel samples were studied by a temperature sweep experiments where the storage modulus was probed under temperature scan at fixed frequency of 1 rad s^{-1} with temperature ramp of 1 ^{0}C/ min. Heating the coacervate and gel samples resulted in decrease of the viscoelastic modulus G', and an sharp change in this decrease indicated a characteristic structure melting temperature T_m. The typical data shown in Fig.4,

clearly identify where a sharp decrease in the value of G' occurred in both coacervate and gel samples, called this temperature, T_m. The melting temperatures obtained for the coacervate and gel samples were T_m = 22±1 and 26 ± 1 ^{0}C, respectively. Since, β-Lg-GB gels were associated with higher rigidity (G') with higher melting temperature in comparison to β-Lg-GB coacervates.

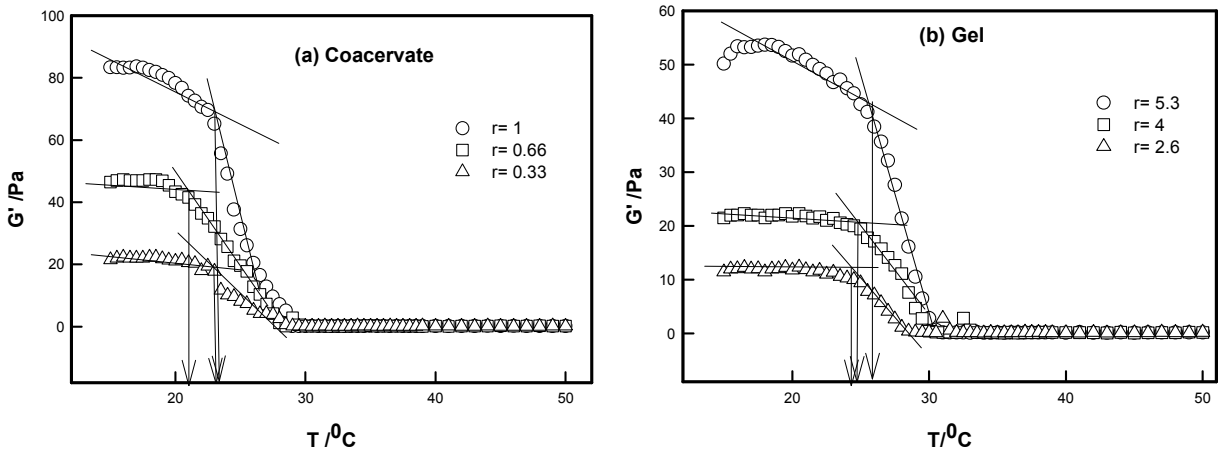

Figure 4: Evolution of storage modulus G′ (ω) for (a) coacervate and (b) gel samples with respect to temperature. Sharp drop indicates a melting temperature (arrows) of samples.

3.2. Cole-Cole plot and dispersion homogeneity

In soft matter comprising of multi-component assembly the structure-property relationship is a function of sample homogeneity. In the linear viscoelastic theory, materials exhibit characteristic relaxation which is a manifestation of the mechanical dissipation of energy in the system. In viscoelastic material the homogeneity depends on storage and loss moduli. Typically, in a polymer melt, at very low frequency, viscous behavior is observed, while elastic properties dominate at higher frequencies. Thus, we investigated mixing ratio dependent sample homogeneity in β-Lg and GB (coacervate and gel state) samples and the phase homogeneity in coacervates and gels was determine from Cole- Cole plot where the imaginary part of complex moduli (G") was plotted against of real part (G') of complex moduli. The value of G' and G" in

coacervate and gel samples are different (shown in Fig. 3) and comes from the same way with a constant oscillation stress of 1 Pa, so the scales are different in both samples. In this formalism $G^*(\omega) = G'(\omega) + iG''(\omega)$ and the low and high frequency values are given by G_0 and G_∞ respectively. The Cole-Cole empirical expression is written as [52,53]

$$G^* - G_\infty = \frac{(G_0 - G_\infty)}{[1+(j\omega\tau_{cc})^{1-k}]} \; ; \qquad 0< k <1 \tag{4}$$

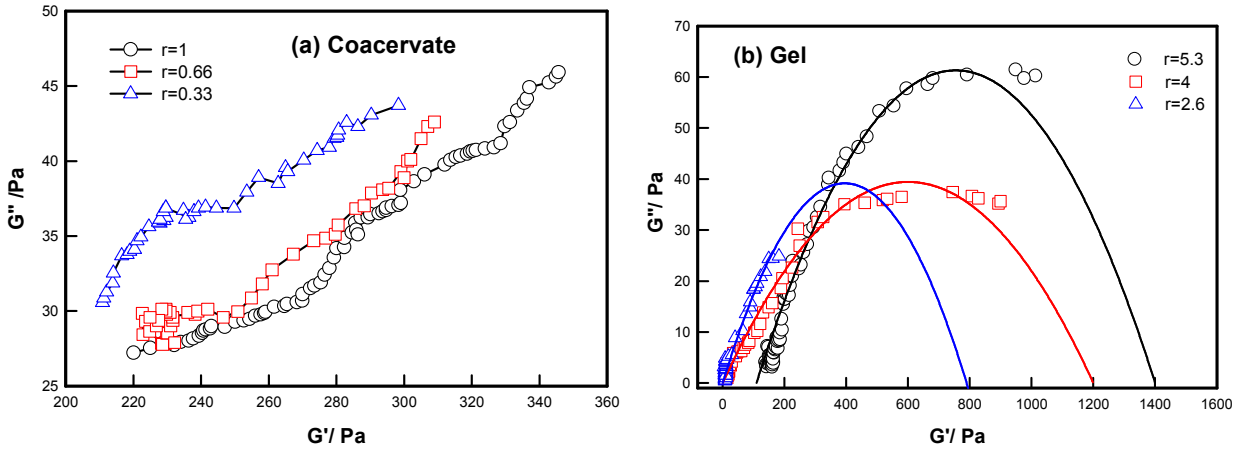

Figure 5: Cole–Cole plot, G" plotted with respect to G' for different mixing ratio (r) with a constant oscillation stress of 1 Pa (a) coacervate samples exhibited strong heterogeneity and (b) gel samples exhibited relatively less heterogeneity. The solid line is the fitting of the data to eq. (4) which could be done for only gel samples.

The Cole-Cole expression in equation 4 is interpreted as arising from a superposition of several Debye relaxation times[54, 55] where τ_{cc} is mean relaxation time of samples. This Cole-Cole plot has been used extensively to determine the map homogeneity of gel and coacervate both samples. For a homogeneous phase, the Cole–Cole plot is a perfect semicircle (k = 0) with a well-defined relaxation time τ_{cc} whereas any deviation from this semicircle shape indicates non-homogeneous dispersion and phase segregation due to immiscibility. The phase homogeneity of coacervate and gel materials was deduce from Cole-Cole plot (G' plotted as a function of G").

The fitted equation arises from the superposition of several Debye relaxations in the complex plains that define a circular arc, and with the exponent parameter k describing the viscoelastic homogeneity of the sample (see Table 1). References 50 and 51 provide further details about the Cole-Cole plot.

Table 1: The τ_{cc} is mean relaxation time and the exponent parameter k, which takes a value between 0 and 1, allows clear definition of sample homogeneity.

Samples	k	τ_{cc} /s
r=2.6	0.43	0.88
r=4.0	0.30	0.91
r=5.3	0.02	0.87

The curves in figure 5(a) show linear behavior, and could not be fitted to eq 4 while data in figure 5(b) was fitted to eq 4 (as a representation fitting for r=1 and 2.6 data are depicted in Figure S2, Electronic Supplementary Information, ESI). Well defined relaxation times and smaller k-values obtained were indicative of the near semicircular feature of the plots implying dispersions were homogeneous (Fig 5(b)). Figure 5 shows that there was homogeneity present in all gel samples whereas inhomogenity was noticed in propensity in coacervate samples because in coacervate samples, these Cole-Cole plots diverged from a semicircle strongly and showing a linear behavior. Here, τ_{cc} value is the inverse of the angular frequency at which G" showed maxima, which referred to the mean viscoelastic relaxation time. The viscoelastic relaxation prevailed over comparable time scales.

3.3 . Kinetics and Relaxation dynamics of gels

In DLS, the intensity- intensity correlation function $g_2(q, t)$, defined as $< I(q,0)I(q, \tau) > /< I(q) >^2$, in the homodyne mode or self- beating mode was measured, where $<I(q, \tau)>$ is time-averaged scattering intensity at time τ with respect to $\tau=0$, that is the measured baseline. Thus $g_2(q, \tau)$ is related to $g_1(q, \tau)$ by the Siegert relation as[56, 57]

$$g_2 (q, \tau) = A[1+ \beta |g_1(q, \tau)|^2] \quad (5)$$

where A is measured baseline and β is a coherence factor depending on instrumental parameters (pinhole size and distance from the detector etc.) For mono-dispersed spherical scatters, $|g_1 (q, \tau)|$ is theoretically represented as an exponential decay function [58,59]

$$|g_1(q, \tau)| = G(q) \exp(-\Gamma\tau) \quad (6)$$

where G and Γ are the factors of proportionality and the linewidth, respectively, and $\Gamma= 1/\tau_r$. The characteristic decay time τ_r represents the rate of dynamic relaxation of concentration fluctuations. For the polydispersed samples the dynamic relaxation, equation (6) may be generalized as [58, 59]

$$|g_1(q, \tau)| = \int_0^\infty G(q, \Gamma)\exp(-\Gamma\tau)d\Gamma \quad (7)$$

where G (Γ) is the distribution function of characteristic decay rate Γ. G (Γ) was calculated from Laplace inversion on the basis of equations (6) and (7). In this study, the CONTIN [58] (constrained regularization method) program supplied with the correlate was used to obtain G(Γ) from $g_1 (q, t)$.

The temporal evolution of correlation function of gelling sols is depicted in Figure 6 where the data pertains to observations taken at $\theta = 90°$. It was observed that as the gel state was

approached the correlation functions did not relax to the equilibrium value (onset of non-ergodicity). In 1% GB system there is no gel formation but at 2%, 3% and 4% GB the base line of time-intensity correlation functions changes which can be interpreted as a superposition from the collective diffusion mode (caused by slightly cross- linked cluster and sol molecule) and the cluster mode (caused by large connected gel cluster) [61, 62]. These features agree with the fact that sol-gel transition takes place.

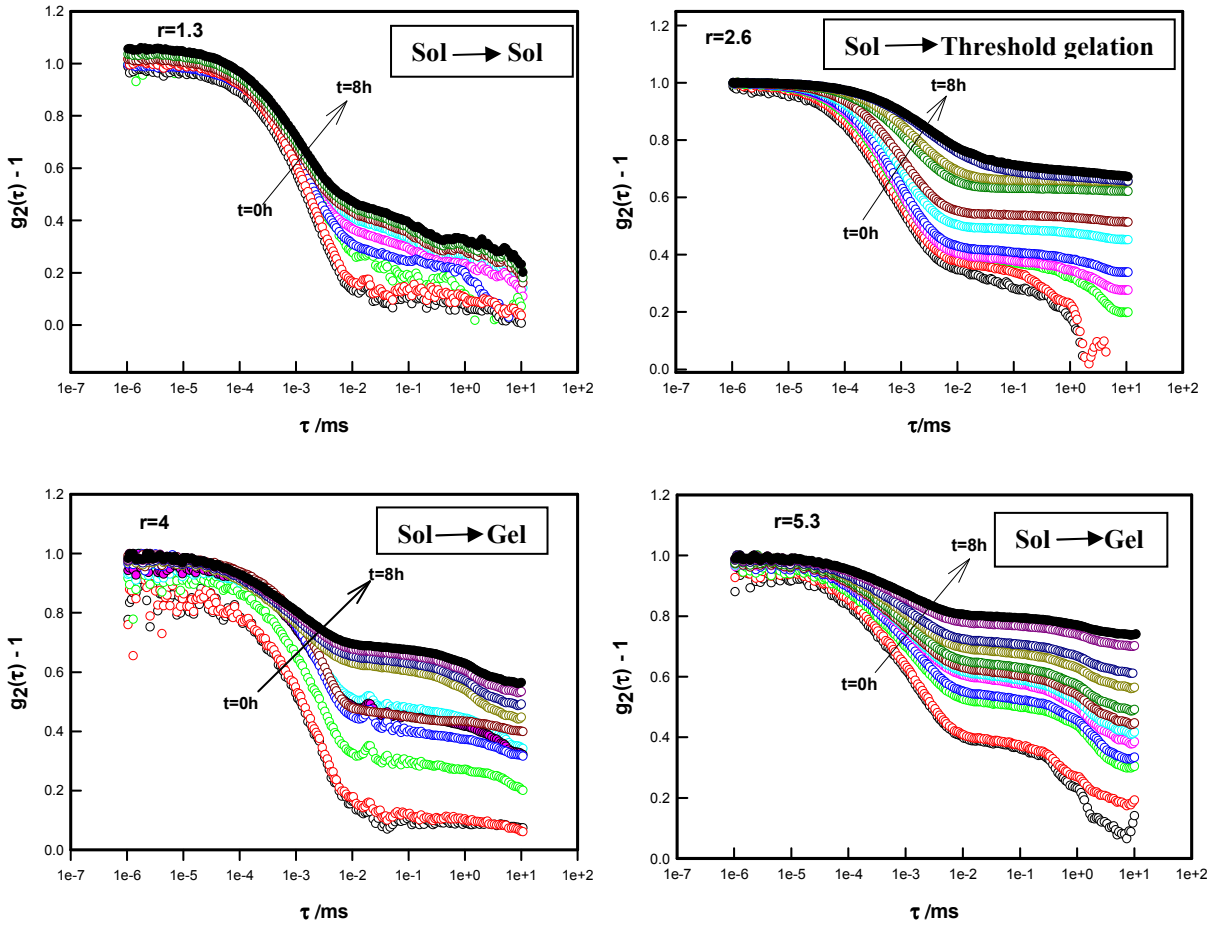

Figure 6: The evolution of dynamic structure factor of the samples with r=1.3, 2.6, 4.0 and 5.3. The arrow indicates the evolution of dynamic structure factor starting t=0h to t=8h.

Figure (6) shows the temporal evolution of [g_2 (q, τ)-1] for, the samples with r=1.3, 2.6, 4.0 and 5.3. Each plot shows similar temporal evolution dynamics. It is clearly seen that the [g_2(q, τ)-1]

did not completely relax as the gelation time increased indicating system was to the arrested phase. For r = 1.3, [g_2 (q, τ)-1] did not changed very much but for r = 2.6, 4.0 and 5.3 samples, the decay of relaxation was slower. This clearly implied onset of dynamics arrest of fluctuations due to confinement of the network units arising out of extensive cross linking.

Figure 7 shows the decay rate distribution functions, $G(\Gamma)$, as a function of characteristic decay rate for sol and gel samples which is obtained from the inverse Laplace transform of $g_2(\tau)$ using the CONTIN algorithm. In sol state the distribution function $G(\Gamma)$ was associated with one single peak, which is shifted towards the small relaxation time. The distribution function $G(\Gamma)$ split into two peaks as system goes from sol to gel phase. That is, the former (sol stage) arising from the translational diffusion of β-Lg-GB system, while the latter (gel stage) was due to the collective diffusion of gel network. In 1%GB system $G(\Gamma)$ for the different reaction time has a single peak. This indicates no phase transition at this stage. In 2%, 3% and 4% GB there is single peak in $G(\Gamma)$ in solution phase but if we increase waiting time, at a certain time G (Γ) split into two peaks, this indicates that the system goes from ergodic to non ergodic phase, called gelation time.

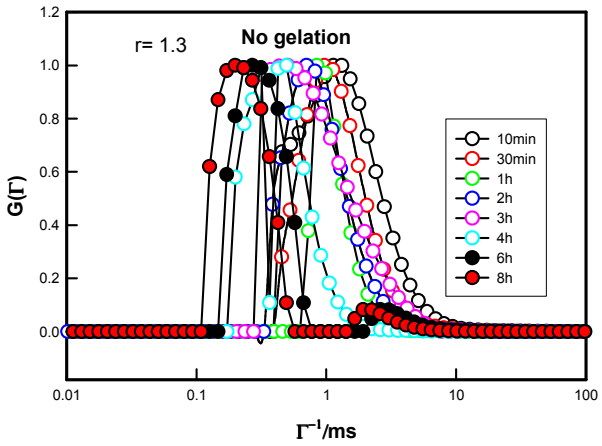

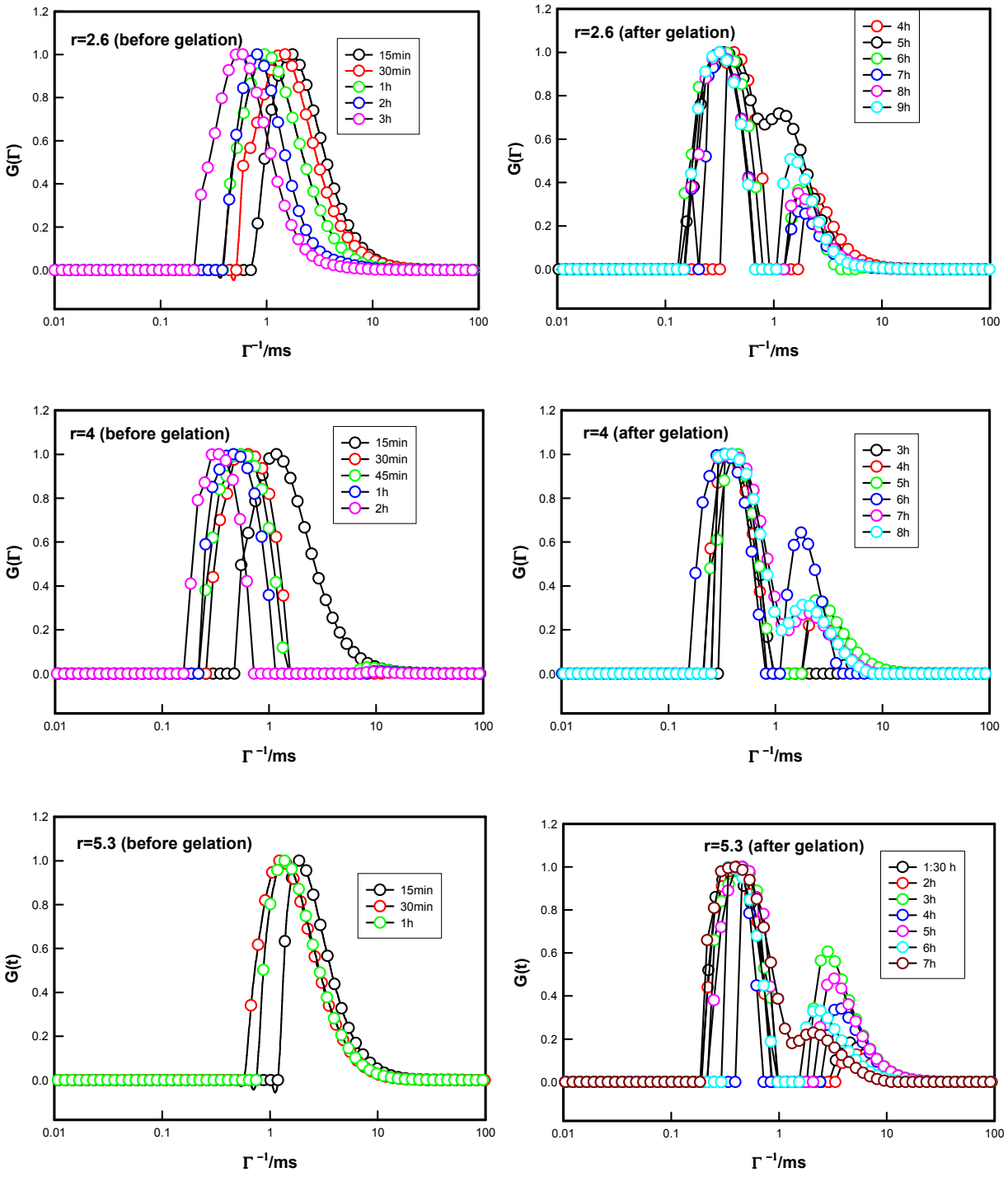

Figure 7: Variation of decay rate distribution functions obtained for samples with r=1.3, 2.6, 4.0 and 5.3 before and after gelation as a function of time.

3.4. Non-Ergodicity and gelation

DLS has been applied to follow the gelation or non-ergodicity of soft systems. In ergodic system the intensity correlation function g_2 (t) can be correlated directly to the corresponding dynamic structure factor g_1(t) via the Siegert relation but in non ergodic system g_2 (t) cannot be correlated directly to the corresponding g_1(t) via Siegert relation. Complication are caused when the scattering moiety in the dispersion medium are localized near fixed mean position and are able only to execute limited Brownian motion about the same. A completely ergodic system is one where the time and ensemble average are identical and the system is independent of the origin of time. The issue of non-ergodicity and its effect on g_2 (q, t) has been addressed adequately in the past. In this work, we adopt the heterodyne approached to resolve the issue of non-ergodicity in our data analysis.

In non-ergodic system the intensity correlation function g_2 (q, t) measured by the correlator can be related to dynamic structure factor through the general expression [63, 64]

$$g_2(q, t) = 1 + \beta[\, 2\chi(1-\chi)\,|g_1(q,t)| + \chi^2\,|g_1(q,t)|^2\,] \qquad (8)$$

Where β is the coherence factor having maximum value β=1. In a real experiment it defines the signal modulation which is a measure of signal-to –noise ratio of the data. The parameter χ ($0 \leq \chi \leq 1$) defines the heterodyne contribution present in the measured g_2(q, t) data. In the sol state χ =1 and the Siegert relationship [$g_2(q, t) = 1 + |g_1(q,t)|^2$] get established. However, in the gel state $\chi < 1$ and the term [2χ (1-χ)] makes a finite contribution to g_2(q, t) . The value of χ can be determined experimentally from the intercept of the plot of [g_2(q, t) -1] versus delay time t at $t \rightarrow 0$ gives β[2χ(1-χ)] from which the value of χ can be calculated if β is known. For an ergodic system, the g_2 (q, t) function relaxes to 0 (at $t = \infty$) from its initial value 1 (t = 0). Thus, the signal

modulation β achieved from the relation $[g_2(q, t)|_{t\to 0} - g_2(q, t)|_{t\to\infty}]$. For a non-ergodic system, β-values lies between 0 and 1. This happens because of the dynamic arrest of the scattering moiety, and this has been observed in a variety of soft matter systems like polymer solutions, colloidal gels, glasses, and so on[65-67].

Figure 7a shows the variation of χ with time at different mixing ratio for gelling sols. In sol state, for r = 1.3, we measured χ = 0.9±0.1. Hence $g_1(q, t)$ could be determined from $g_2(q, t)$ data directly, using Seigert relation. In the gel state χ decreased with time and remained constant after the gelation was achieved. Thus, we could neglect the contribution of second term in equation (8) and fit the data to evaluate the various relaxation modes explicitly. This allows us to define an ergodicity breaking time, τ_{EB}. This is the time beyond which the ergodicity of the sample does not change Interestingly, It determines the gelation time of the samples. Figure 7(b) shows the t_g (from DLS and rheology) and ergodic breaking time τ_{EB} as a function of r, which indicates that the value of gelation time is exactly matches with the ergodicity breaking time. The concentration of GB strongly affects the gelation kinetics, and network becomes stronger with an increase in the GB concentration (confirmed from the viscoelastic data). At high mixing ratio the network becomes denser with increase in GB concentration with the β-Lg aggregating on GB chains. Due to abundance of GB chains the gelation process is enhanced and the difference between gelation time and ergodic breaking time becomes smaller, while at low mixing ratio abundance of GB is low so the difference between the gelation time and ergodic breaking time becomes more.

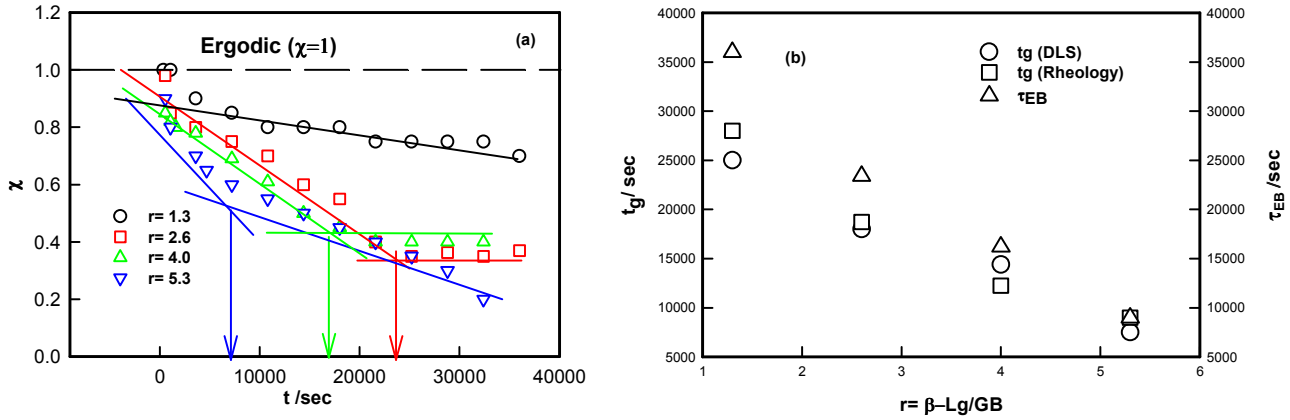

Figure 8: (a) The heterodyne contribution χ shown as a function of ageing time t/sec. the point where there is slop changes in the value of χ is defined as a ergodicity breaking time τ_{EB}. (b) The ergodicity breaking time τ_{EB} and gelation time of samples as a function of mixing ratio r from DLS and rheology.

3.5. Phase diagram

We proposed a phase diagram in Figure 9 using zeta potential versus temperature a variable to describe all the physical expected features observed in this study. The conceptual understanding developed for the all samples with respect to mixing ratio (r), and heat-induced phase transitions were summarized as follows: In Phase-I for r ≥ 1.0, the interaction between protein and polyampholyte occurred marginally above the isoelectric point (pI) of protein where the protein being overall positively charged and a cloudy solution was formed, this indicating formation of soluble intermolecular complexes (coacervation). Here, the charge neutralized intermolecular complexes were formed due to strong surface patch binding between both biopolymers. In the phenomena of surface patch binding, these charged patches are opposite in sign to the net protein (β-Lg) charge, could provide sites for binding to polyampholyte (GB) chain with the same charge sign as protein. In Phase-II, i.e. for r ≤1, the interaction between protein and

polyampholyte occurred slightly below the isoelectric point (pI) of protein where the protein being overall negatively charged and the mixture remained homogeneous and there is no indication of either intermolecular soluble complex formation (turbidity) or phase separation. This dispersion turned into a gel-like phase over a period of time and network formation in these samples were mostly due to hydrogen bonding between flexible gelatin chains with β-Lg acting as binding units. Due to the presence of β-Lg molecule, this network was very weak in comparison of GB network formed at same concentration because this was which was attached to the GB chains causing network deformations whereby weak gels were formed.

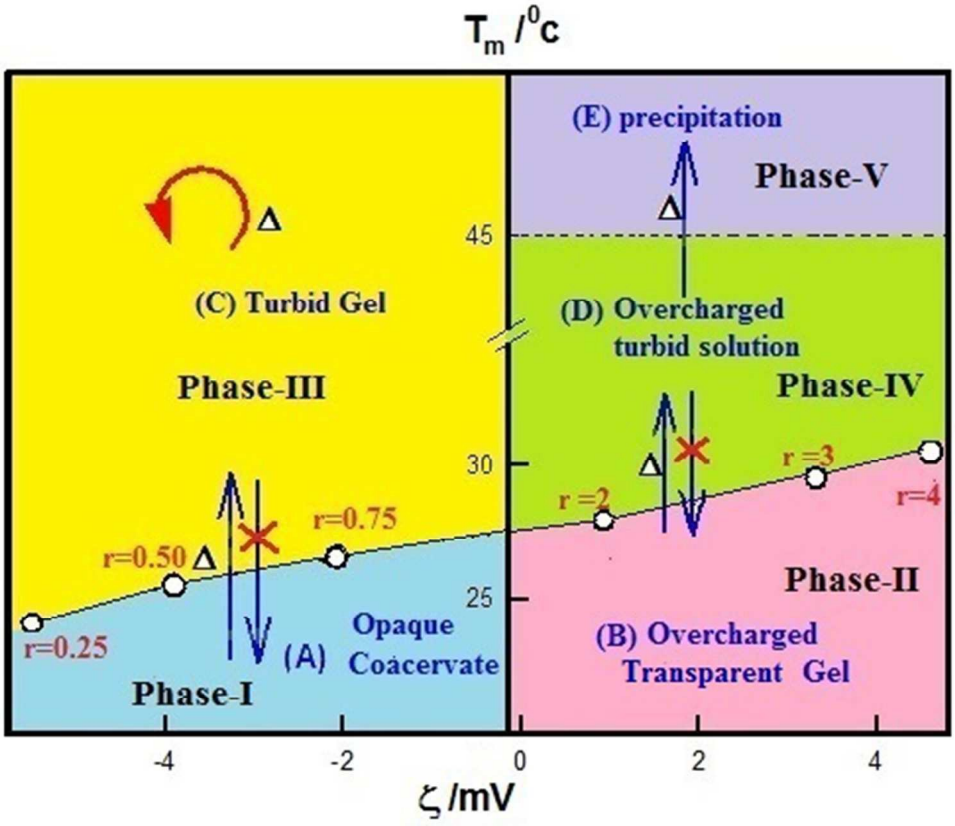

Figure 9: Typical Phase diagram of various soft matter states in β-Lg-GB complexation, r = [GB]: [β-Lg] as a function of surface charge and melting temperature.

All coacervate samples are opaque in nature, when these coacervate samples (**Phase-I**) were subjected to slow heating (1 ^{0}C/min) in a thermostat up to a maximum temperature 45 ^{0}C and then followed by gradually cooling to room temperature (20 ^{0}C). During this procedure, the originally opaque looking all coacervate samples on heating became turbid sol that turned into gel-like network after an equilibration time of 24 hours (**Phase-III**). Similarly when the all overcharged transparent gel samples **(Phase-II)** were subjected to slow heating (1 ^{0}C/min) in a thermostat up to a maximum temperature 45 ^{0}C followed by gradual cooling to room temperature (20 ^{0}C), these changed into overcharged turbid solution **(Phase-IV).** The high turbidity was seen in these samples, which is due to the nature of thermal aggregation of protein (β-Lg). It is to be noted that if these overcharged gels (**Phase-II**) were heated beyond 45 ^{0}C, these samples immediately precipitated with gradual cooling to room temperature (**Phase-V**).

4. Conclusions

We studied the interaction between β-Lg and GB mixed in different weight ratio and find that associations were mainly due to surface patch binding. For $r < 1.0$ there was formation of turbid solution with indication of soluble complex formation or phase separation (coacervation). For $r > 1.0$, the dispersion obtained homogeneous and there is no indication of either intermolecular complex formation or phase separation. This dispersion turned into a gel-like phase over a certain period of time. In this study, to observe gelation processes of β-Lg–GB dispersions were monitored by rheology as a function of the β-Lg –GB mixing ratio. The frame of gel organization was found in flexible GB chain while the β-Lg aggregated along the GB chains and could be regarded as a cross linking agent, and If we increase the GB concentration the viscoelasticity of gels is also increased. The zeta potential and absorbance data showed that there

was partial charge neutralization in the region of r < 1, called coacervation regime, and in the region of r > 1 overcharging and gel-like network formation dominated.

The systematic rheology studies of both phases (gels and coacervates) show viscoelastic nature. G_0 is the measure of rigidity of a network. In the region of r < 1.0, G_0 was greater than r > 1.0 also the melting temperature of gels was higher than coacervates, which indicated gels were stiffer than coacervates. From rheology data, we have shown that sol-gel transitions are observed with time and define a characteristic parameter t_g, was the time required for the system to get arrested. From the Cole-Cole plot there is homogeneity observed in gel phase.

In the study of DLS shows typical β-Lg-GB solution dynamics in the time-correlation function is observed from the beginning of the reaction up to gelation time. The decrease in the time correlation function can be interpreted as a superposition from the collective diffusion mode (caused by slightly cross-linked both sol molecules) and the cluster mode (caused by formed larger connected gel network). This indicates sol-gel phase transition in systems. We will discuss the relaxation dynamics of relaxation modes of β-Lg-GB molecules occurring in solution and gel phase observed at different mixing ratio. On increasing aging time the system moved towards ergodic to non ergodic medium. At initial time when the system is in dilute region only one mode observed which is due to the system towards ergodic phase owing to faster Brownian dynamics. After a certain time, single internal mode turns into one fast and one slow relaxation mode which is due to new dynamical process involving interchain interaction and disentanglement begin to occur besides the fast relaxation mode. This certain time was time required for the system to get arrested which is approximately same as rheological observation. Finally, draw heat induced phase diagram of different heat induced stages of β-Lg-GB system in the absence of added salt.

The intermolecular interactions prevailing in coacervate and gel phase are mostly due to surface patch binding and hydrogen bonding. In coacervate phase (r>1) charge neutralization occurs due to surface patch binding between β-Lg and GB. In gel phase (r<1) due to large amount of overcharged complexes present, the interaction was mostly due to intermolecular hydrogen bonding between gelatin chains. The simplest molecular mechanism describing different phase transitions in β-Lg-GB system is remarkably similar to BSA-GB system which is described in reference 2 (Figure 12 of reference 2). The following Table 2 provides a comparison between two pairs of interacting proteins having common pI. More detail of these systems is found in reference 2[#] and reference 4*.

Table 2: A comparison between two pairs of interacting proteins (BSA-GB & β-Lg-GB) having common pI.

Techniques/Parameter	BSA-GB	β-Lg-GB	Comments
Fluorescence Binding constant/M^{-1}	162±0.15*	43±0.01*	Binding constant of BSA-GB >β-Lg-GB.
FRET (Energy transfer Efficiency E %)	63%*	30%*	BSA-GB indicates energy transfer efficiency of BSA-GB > β-Lg-GB.
Rheology G'/Pas	150±50(r<1)[#] 130±10(r>1)	135±50 (r<1) 100±50 (r>1)	Gel strength of BSA-GB > β-Lg-GB.
T_m/^{0}C	30±1 (r<1) [#] 33±1 (r>1)	22±1 (r<1) 26±1 (r>1)	Melting temperature of BSA-GB> β-Lg-GB.

Acknowledgments JP acknowledges University Grants Commission, Government of India for a Junior Research Fellowship. KR acknowledges DST-Inspire Faculty Award from Department of Science and Technology (DST), Government of India. This work was supported by a research grant from DST.

Supporting Information (SI)

UV-Vis absorbance spectra and Cole–Cole plot for different mixing ratios of β-Lg and gelatin B undertaken in this study are included in the Supplementary information.

References

1. Y. Xu, D. Seeman, Y. Yan, Lianhong Sun, Jared Post and Paul L. Dubin, *Biomacromolecules*, 2012, **13**, 1642-1651.
2. J. Pathak, K Rawat, V. K. Aswal and H. B. Bohidar, *J. Phys. Chem. B*, 2014, **118(38),** 11161-71.
3. C. Stuart, *Langmuir*, 2004, 20, 2785–2791. And M. Skepoe and P. Linse, *Macromolecules*, 2003, 36, 508–519.
4. J. Pathak, K Rawat, V. K. Aswal and H. B. Bohidar, *RSC Adv.*, 2015, **5**, 13579-13589.
5. Y. Murakami and S. Jones, *Structural bioinformatics* 2006, **22 (14),** 1794–1795.
6. M. Lund, L. Vrbka, and P. Jungwirth , *J. Am. Chem. Soc*., 2008, **130**, 11582–11583.
7. B. Kayitmazer, D. Seeman, B. B. Minsky, P.L. Dubin and Y. Xu, *Soft Matter*, 2013, **9**, 2553–2583.
8. J. van der Gucht, E. Spruijt, M. Lemmers and M.A. Cohen Stuart, *J. Colloid Interface Sci.,* 2011, **361**, 407–422.
9. P. Maarten, M. A. Biesheuvel, F. M. Menger and B.M. Sykes, *Langmuir*, 1998, **14**, 4131–4137.
10. E. Tsuchida and K. Abe, *Inter Macromolecular Complexes, Springer*, Heidelberg, Germany, 1982.

11. H. G. Bungenberg de Jong, in: H.R. Kruyt (Ed.), *Colloid Science*, vol. II, Elsevier, New York, 1949.

12. J. Pathak, K. Rawat and H. B. Bohidar, *Int. J. Biol. Macromols*., 2014, **63**, 29-37.

13. D. Priftis, K. Megley, N. Laugel and M. Tirrell, *J. Colloid Interface Sci.*, 2013, **398**, 39-50.

14. K. Kaibara, E. Seyrek, P. L. Dubin, C. Tribet and E. A. Gamble, *Biomacromolecules,* 2003, **4**, 273-282.

15. E. Kizilay, A. Basak Kayitmazer and Paul L. Dubin, *Adv. Colloid Interface Sci.*, 2011, **167**, 24–37.

16. A. S. Michaels and R. G. Miekka, *J. Phys. Chem*., 1961, **65**, 1765.

17. F. Vongoeler and M. Muthu kumar, *J. Chem. Phys.,* 1994, **100,** 7796.

18. M. Girard, S. L. Turgeon and S. F. Gauthier *J. Agric Food Chem.,* 2003, **51**, 4450.

19. X. Feng, M. Leduc and R. Pelton, *Colloids Surf. A,* 2008, **317**, 535.

20. V. Ball and C. Maechling *Int. J. Mol. Sci.,* 2009, **10**, 3283.

21. D. Leisner and T. Imae, *J Phys. Chem. B,* 2003, **107**, 8078.

22. A. Veis, *Adv. Colloid Interface Sci ,* 2011, **167**, 2–11.

23. J. Overbeek and M. J. Voorn, *J. Cell. Comp. Physiol.,* 1957, **49**, 7.

24. A. Veis, *J. Phys. Chem.,* 1963, **67 (10),** 1960–1964.

25. A. Veis, *J. Phys. Chem.,* 1798, **65**, 1961.

26. A. Nakajima , and H. Sato, *Biopolymers*, 1972, **10**, 1345.

27. K. Tainaka, *Biopolymers,* 1980, **19**, 1289.

28. A. Basak Kayitmazer , Daniel Seeman , Burcu Baykal Minsky , Paul L. Dubin and Yisheng Xu, *Soft Matter*, 2013, **9**, 2553-2583.

29. J. M. Park, B. B. Muhoberac, P. L. Dubin and J. Xia, *Macromolecules*, 1992, **25**, 290–295.

30. J. Gao, P. L. Dubin and B. B. Muhoberac, *J. Phys. Chem. B*, 1998,**102**, 5529–5535.

31. C. Schmitt, C. Sanchez, A. Lamprecht, D. Renard, C.M. Lehr, C.G. de Cruif and J. Hardy, *Colloids Surf. B*, 2001, **20**, 267–280

32. C. Sanchez, G. Mekhloufi, C. Schmitt, D. Renard, P. Robert, C.-M. Lehr, A. Lam-phret and J. Hardy, *Langmuir*, 2002, **18,** 10323–10333.

33. F. Weinbreck, R. H. Tromp and C. G. de Cruif, *Biomacromolecules*, 2004, **5**, 1437–1445.

34. F. Weinbreck, H. S. Rollema, R. H. Tromp and C. G. de Cruif, Langmuir, 2004, **20**, 6389–6395.

35. A. N. Gupta and H.B. Bohidar, *J. Phys. Chem. B*, 2007, **111,** 10137–10145.

36. S. Boral and H.B. Bohidar, *J. Phys. Chem. B*, 2010, **114,** 12027–12035.

37. A. Tiwari, S. Bindal and H. B. Bohidar, *Biomacromolecules,* 2009, **10**, 184–189.

38. K. Rawat, V.K. Aswal and H.B. Bohidar*, J. Phys. Chem. B,* 2012, **116**, 14805–14816.

39. Y. Wang, Y. Li, Y. W. Wang, J. Lal and Q. Huang, *J. Phys. Chem. B*, 2006, **111**,515–520.

40. Wang, J. Y. Gao and P. L. Dubin, *Biotechnol. Prog*., 1996, **12**, 356−362.

41. P. L. Dubin, S. S. The, D. W. Mc Quigg, C. H. Chew and L.M. Gans, *Langmuir,* 1989, **5***,* 89−95.

42. A. B. Kayitmazer, H. B. Bohidar, K. M. Mattison, A. Bose, J. Sarkar, A. Hashimoto, P. S. Russo, W. Jaeger and P. L. Dubin, *Soft Matter,* 2007, **3**, 1064−1076.

43. K. Kaibara, T. Okazaki, H. B. Bohidar and P. L. Dubin, *Biomacromolecules*, 2000, **1**, 100−107.

44. H. Ohshima, *Adv. Colloid Interface Sci*., 1995, **62**, 189−235.

45. B. Mohanty and H. B. Bohidar, *Biomacromolecules*, 2003, **4**, 1080-1086.

46. H. A. Barnes, Handbook of Elementary Rheology; University of Wales Press: Wales, 2000.

47. B. Mohanty, A. Gupta, H. B. Bohidar and S. Bandyopadhyay, *J. Polymer Science: Part B: Polymer Physics,* 2007 **45**, 1511–1520.

48. J. E. Martin, D. Adolf, J. P. Wilcoxon, *Phys. Rev. Lett*., 1988, **61**, 2620−2623.

49. J. E. Martin and D. Adolf, *Annu. Rev. Phys. Chem,.* 1991, **42,** 311−339.

50. H. H. Winter and F. J. Chambon, *J. Rheol*., 1986, 30, 367–382.

51. H. A. Barnes, Handbook of Elementary Rheology, University of Wales, Wales, 2000.

52. N. Arfin and H. B. Bohidar, *Int. J. Biol. Macromol.*, 2012, **50**,759–767.

53. K. S. Cole and R. H. Cole, *J. Chem. Phys*., 1941**, 9,** 341–351.

54. T.C. Warren, J. L. Schrag and J. D. Ferry, *Biopolymer,* 1973 **12**, 1905-9015.

55. Q. Zheng, M. Du, B. B. Yang and G. Wu, *Polymer,* 2001, **42,** 5743-5747.

56. H. Z. Cummins, E.R. Pike. *Photon Correlation and Light Beating Spectroscopy*, Plenum, New York, 1974.

57. B. Chu. *Laser Light Scattering*, Academic Press, New York, 1974.

58. B. J. Berne and R. Pecora., *Dynamic Light Scattering*, Wiley-Inter-science, New York, 1976.

59. R. J. Glauber, *Quantunm Optics and Electronics*, Gordan and Breach, New York, 1965.

60. S. W. Provencher, *Comput. Phys. Commun*. 1982, **27**, 213 (b) *ibid* **27**, 229 (1982).

61. T. Tanaka, R. Pecora, Dynamic *Light Scattering*, and Plenum Publishing: New York, 1985, 347.

62. M. Shibayama, Y. Isaka and Y. Shiwa, *Macromolecules* 1999, **32**, 7086.

63. k. Te. Nijenhuis, (See the example) *Thermo-reversible network: Advances in Polymer Science*, 1997, **130**, 1-7.

64. J. Sharma, and H. B. Bohidar, *Europ. Poly. J.,* 2000, **36**, 1409-1418 and ibid *colloid and polym. Sci.,* 2000, **278**, 15-21.

65. B. Ruzicka, E. Zaccarelli, L. Zulian, R. Angelini, M. Sztucki, A. Moussaid, T. Narayanan and F. Sciortino, *Nat. Mater*., 2011, **10**, 56−60.

66. P. N. Segre, V. Prasad, A. B. Schofield and D. A. Weitz, *Phys. Rev. Lett*., 2001, **86 (26),** 6042−6045.

67. L. D. Michele, F. Varrato, J. Kotar, S. H. Nathan, G. Foffi and E. Eiser, *Nat. Commun*., 2013, **4**, 2007.